ADVANCED FUNCTIONAL MATERIALS
www.afm-journal.de

Organic Solar Cells: Electrostatic Stabilization of Organic Semiconductor Nanoparticle Dispersions by Electrical Doping

*Felix Manger, Philipp Marlow, Karen Fischer, Manuel Nöller, Christian Sprau, and Alexander Colsmann**

Organic semiconductor nanoparticle dispersions are electrostatically stabilized with the p-doping agent 2,3,5,6-tetrafluoro-7,7,8,8-tetracyanoquinodimethane (F_4TCNQ), omitting the need for surfactants. Smallest amounts of F_4TCNQ stabilize poly(3-hexylthiophene) dispersions and reduce the size of the nanoparticles significantly. The concept is then readily transferred to synthesize dispersions from a choice of light-harvesting benzodithiophene-based copolymers. Dispersions from the corresponding polymer:fullerene blends are used to fabricate organic solar cells (OSCs). In contrast to the widely used stabilizing surfactants, small amounts of F_4TCNQ show no detrimental effect on the device performance. This concept paves the way for the eco-friendly fabrication of OSCs from nanoparticle dispersions of high-efficiency light-harvesting semiconductors by eliminating environmentally hazardous solvents from the deposition process.

1. Introduction

The solution-processability of organic semiconductors enables the fast and flexible design of organic optoelectronic devices and eventually their production by large-scale high-throughput printing and coating. As of today, most organic semiconductors are only soluble in halogenated, aromatic, or heterocyclic solvents such as chloroform, chlorobenzene, or tetrahydrofuran. Unfortunately, the environmental and health hazards of these solvents[1–3] require the implementation of expensive solvent capturing techniques which are in conflict with low production costs. In particular, in the field of organic solar cells (OSCs), substantial research efforts have been conducted toward replacing these solvents with non-toxic, environmentally friendly solvents.[4,5] Significant progress has been achieved over the last years by modifying high-performance organic semiconductors to enhance their solubility in tetrahydrofuran, *o*-xylene, or toluene, eliminating halogenated solvents while maintaining the high power conversion efficiencies (PCEs) of the corresponding solar cells beyond 17%.[6–8] An alternative route toward eco-friendly processing agents, such as water or alcohol, is the synthesis of nanoparticle inks. Light-harvesting layers for solar cells can then be fabricated from nanoparticle dispersions by the same deposition methods used for solvent processing (spin coating, doctor blading, and inkjet printing).[9] After deposition, thermal annealing warrants the joining of the nanoparticles and the formation of a closed layer.[10] While virtually any organic semiconductor can be dispersed in suitable agents at low concentrations, for example, for spectroscopic investigations,[11] the fabrication of OSCs requires dispersions with high concentrations in the g L^{-1} regime, often causing the coagulation of the dispersions. Highly concentrated dispersions can only be achieved if they are strongly stabilized against coagulation.

Ionic surfactants have been widely used to stabilize aqueous organic semiconductor nanoparticle dispersions prepared by the miniemulsion method.[12–14] Yet, these surfactants remain in the bulk-heterojunction where they are suspected to hinder charge carrier transport and thus reduce the performance of the OSCs.[14–17] Moreover, the slow formation of nanoparticles in miniemulsions promotes the formation of core–shell structures, which may also be detrimental to the later performance of solar cells. Yet, tailoring the nanoparticle morphology between core–shell, intermixed, and flipped core–shell architectures in miniemulsion processes was achieved by controlling the surface energy.[18]

In earlier work, the drawbacks of employing surfactants, that is yielding core–shell nanoparticles and wetting issues with water during later thin-film deposition, prompted us to synthesize surfactant-free nanoparticle dispersions from blend solutions of poly(3-hexylthiophene) (P3HT) and indene-C_{60}

F. Manger, P. Marlow, K. Fischer, M. Nöller, C. Sprau, A. Colsmann
Material Research Center for Energy Systems (MZE)
Karlsruhe Institute of Technology (KIT)
Strasse am Forum 7, 76131 Karlsruhe, Germany
E-mail: alexander.colsmann@kit.edu

F. Manger, P. Marlow, K. Fischer, M. Nöller, A. Colsmann
Light Technology Institute
Karlsruhe Institute of Technology (KIT)
Engesserstrasse 13, 76131 Karlsruhe, Germany

The ORCID identification number(s) for the author(s) of this article can be found under https://doi.org/10.1002/adfm.202202566.

DOI: 10.1002/adfm.202202566

bisadduct (ICBA) by nanoprecipitation in alcohols, yielding dispersions with remarkable shelf-stability and OSCs with PCEs of 4%.[10] The principal nanoprecipitation method by solvent displacement was first described by Takeuchi.[19,20] If a polymer solute in a good solvent is injected into an excess amount of a miscible non-solvent, the immediate change in solubility supersaturates the solution, causing the polymer chains to collapse and eventually form nanoparticles.[21] In contrast to the slow nanoparticle formation in miniemulsion processes, the rapid nanoparticle formation during nanoprecipitation promotes well-intermixed polymer and fullerene phases inside the nanoparticles.[22] So far, only very few organic semiconductors have formed stable nanoparticle dispersions upon nanoprecipitation, with the most prominent examples being P3HT, as well as blends of P3HT and fullerenes. To enable the use of other semiconducting polymers, Xie et al. added a sterically stabilizing poloxamer to the nanoprecipitation process, but laborious subsequent cleaning steps were necessary to iteratively reduce the surfactant content for best photovoltaic performance.[17]

Electrostatic effects were reported to stabilize nanoparticles of individual polymers.[23] And recently, we reported that the intrinsic stability of P3HT and P3HT:ICBA nanoparticle dispersions is also of electrostatic origin.[24] If electrostatic effects are powerful enough to stabilize P3HT:ICBA nanoparticles over an extended period of time, the deliberate generation of (surface) charges on the nanoparticles should enhance the colloidal stability. A common approach to charge organic semiconductors is electrical p-doping with strong oxidizing agents such as 2,3,5,6-tetrafluoro-7,7,8,8-tetracyanoquinodimethane (F_4TCNQ).[25–42] In this work, we investigate the stabilization of organic nanoparticle dispersions by electron transfer from the comprised polymer to F_4TCNQ. To present the principal case and for best comparability with the literature, we study the effect of F_4TCNQ on dispersions of P3HT or P3HT:ICBA. Thereafter, we transfer the concept to other organic semiconductors and blends, which are commonly used in OSCs, and which otherwise would immediately show strong coagulation upon nanoprecipitation.

2. Results and Discussion

2.1. Doping of P3HT Dispersions

The principal effect of the dopant F_4TCNQ on organic semiconductor nanoparticles is best studied on the well-known donor-type semiconductor P3HT. P3HT forms stable nanoparticle dispersions in absence of surfactants, which lets us compare the effect of doping with a non-doped reference. F_4TCNQ can undergo an integer charge transfer with P3HT, leaving a positive charge on P3HT, with a doping efficiency on the order of 60%–70% in chloroform.[35]

All P3HT dispersions were synthesized by nanoprecipitation following established experimental protocols.[10] Therefore, we rapidly injected chloroform solutions of P3HT (2 g L^{-1}) into the miscible non-solvent ethanol (1:4 v/v). To investigate the effect of F_4TCNQ-doping on P3HT dispersions, we added F_4TCNQ/acetonitrile solutions (10 g L^{-1}) in small amounts to the P3HT/chloroform solutions prior to nanoprecipitation. The mass ratio of F_4TCNQ and P3HT (w_{F_4TCNQ}) was varied between 0.005 and 5 wt%. The nanoparticles were then formed upon injection of the P3HT:F_4TCNQ solutions into ethanol.

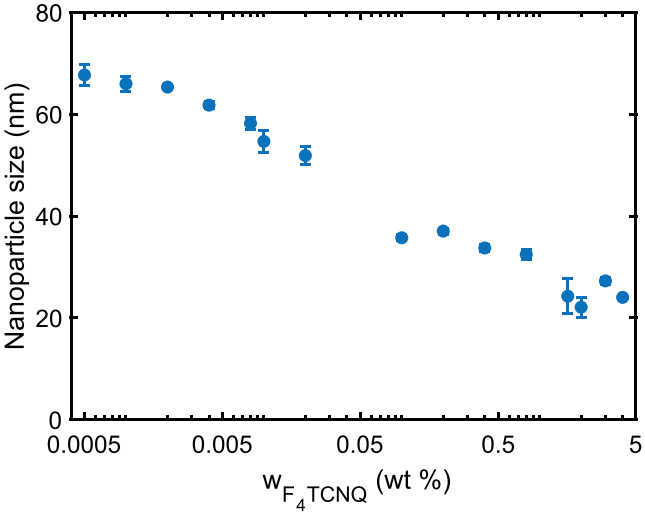

Figure 1. P3HT nanoparticle size after addition of F_4TCNQ/acetonitrile to the P3HT/chloroform solution and subsequent nanoprecipitation versus the mass ratio of F_4TCNQ and P3HT (w_{F_4TCNQ}). The error bars represent the standard deviations of at least three independent experimental results.

The nanoparticles were almost spherical (see atomic force microscopy, AFM, images in Figure S1, Supporting Information). The electrical doping of P3HT nanoparticle dispersions with F_4TCNQ directly affects the size of the nanoparticles in **Figure 1** but not their shape. If no F_4TCNQ is added to the P3HT/chloroform solution before nanoprecipitation (w_{F_4TCNQ} = 0 wt%), the nanoparticles exhibit a size of 72 nm, which is in agreement with earlier works.[22] Even at very low concentrations of w_{F_4TCNQ} = 0.004 wt%, we found a reduction of the nanoparticle size to 62 nm. This concentration of F_4TCNQ corresponds to about 12 F_4TCNQ molecules per nanoparticle (for details see Section S1, Supporting Information). At w_{F_4TCNQ} = 0.1 wt%, the nanoparticle size is further reduced to 36 nm, which is half the nanoparticle size of the non-doped dispersion. Up to w_{F_4TCNQ} = 0.4 wt%, the nanoparticle size steadily decreases, before the effect saturates. This saturation corresponds to a concentration of approximately one F_4TCNQ molecule per P3HT chain (Equation (S2), Supporting Information).

The reduction of the nanoparticle size through electrical doping can be understood by reviewing the fundamental mechanisms of the nanoparticle growth process. During the nanoprecipitation of high-molecular-weight polymers, the individual polymer chains collapse immediately after solvent displacement.[43] The resulting nuclei size is already in the range of the critical nuclei size, and thus the growth process of the P3HT nanoparticles is mainly controlled by their colloidal stability.[44,45] According to the DLVO theory, the colloidal stability of electrostatically stabilized nanoparticle dispersions can be described by the interplay of attractive van der Waals forces and repulsive electrostatic forces, which together form an energy barrier.[46] As both forces increase with nanoparticle size, this energy barrier is increased during nanoparticle growth, until it

is sufficient to prevent further agglomeration. If the repulsive forces are low, the process may not stop at all, leading to continuous growth and hence the rapid formation of visible agglomerates.[47] If the repulsive forces are enhanced, for example, by an increased number of surface charges, the nanoparticle growth stops earlier, leading to smaller nanoparticles.[45,48] Electrical doping with F_4TCNQ adds to the surface charge of the nanoparticles and hence helps to stop nanoparticle growth and to suppress agglomeration. The feasibility of using low dopant concentrations also lets us conclude that, unlike surfactants, surface coverage of the nanoparticles by F_4TCNQ is not the predominant stabilization mechanism.

2.2. The Role of the Counterion

Importantly, the charging of the nanoparticles can only occur if the countercharges are displaced from the nanoparticles. If the countercharges remained on the nanoparticles, the nanoparticles would exhibit zero net charge even after electrical doping. Once an electron from P3HT has been accepted, the F_4TCNQ^- anion must be detached from the nanoparticle and must not be incorporated in order to foster the charging of the nanoparticle. According to earlier literature reports on doping of P3HT in solution, the F_4TCNQ^- anion can be separated more efficiently from the charged P3HT, if the permeability, ε_r, of the environment is high,[31,49] which prompted us to use ethanol ($\varepsilon_r = 24.5$) as the dispersion medium. Moreover, F_4TCNQ exhibits some solubility in ethanol, which facilitates the separation of the F_4TCNQ^- anion from the positively charged nanoparticle.

The F_4TCNQ^- anion has been reported to show distinct absorption features,[30] which allows us the investigation of the dispersion and its ions by UV–vis–NIR spectrometry. **Figure 2**a depicts the optical density of P3HT:F_4TCNQ/chloroform solutions (dashed lines) and the corresponding dispersions after nanoprecipitation in ethanol (solid lines). For reference, the black lines show the absorption of typical neat (undoped) P3HT/chloroform solutions and P3HT/ethanol dispersions, the latter of which exhibit the commonly observed redshift of semi-crystalline P3HT.[50,51] Upon p-doping with F_4TCNQ, we observed the emergence of two distinct spectral features. One of these two features is a broad absorption shoulder between 1.2 and 1.8 eV, which was previously attributed to the electronic transition P2 of polarons in P3HT either by electrochemical oxidation of P3HT or by molecular p-doping.[35,39,52,53] The second feature comprises two absorption peaks at 1.45 and 1.65 eV.[35,39] These two peaks are the fingerprint of the F_4TCNQ^- anion, evidencing the electron transfer to the F_4TCNQ moiety. Toward larger w_{F_4TCNQ}, both features become more pronounced, indicating an overall increase in electrical p-doping by integer charge transfer. Upon nanoprecipitation, that is, the transition from semiconductor solution to dispersion, both the polaron absorption peak P2 as well as the absorption of the F_4TCNQ^- anion persisted. Thus, we infer that the amount of polarons on P3HT also persisted, that is, the previously generated charges still populate P3HT after nanoprecipitation. We note that even the non-doped sample shows a weak P2 feature, which may indicate an intrinsic charging of P3HT and explain the exceptional intrinsic colloidal stability of P3HT nanoparticle dispersions. We further note that in solution, the absorption band at 2 eV was more enhanced toward increased doping ratios, which is generally indicative of a closer packing of P3HT.[54,55] Thus, electrical doping may also affect the packing of P3HT, which in turn would influence nanoparticle formation.

The electrostatic stabilization of the dispersion requires a displacement of the F_4TCNQ^- anion from the nanoparticles. To investigate whether F_4TCNQ^- anions are present in the dispersion medium, we intentionally triggered the coagulation of a representative doped P3HT dispersion (P3HT/chloroform solution, 2 g L^{-1}, doped with F_4TCNQ, w_{F_4TCNQ} = 1 wt%, nanoprecipitated in ethanol, 1:4 v/v) by adding sodium bromide (10^{-3} M), removed the sediments by centrifugation, and measured the optical density of the supernatant, which is displayed in Figure 2b. We then deconvolved the spectrum into the spectra of neutral, anionic, and dianionic F_4TCNQ with a least-square fit. The best fit was achieved if all F_4TCNQ molecules were in their anionic form.

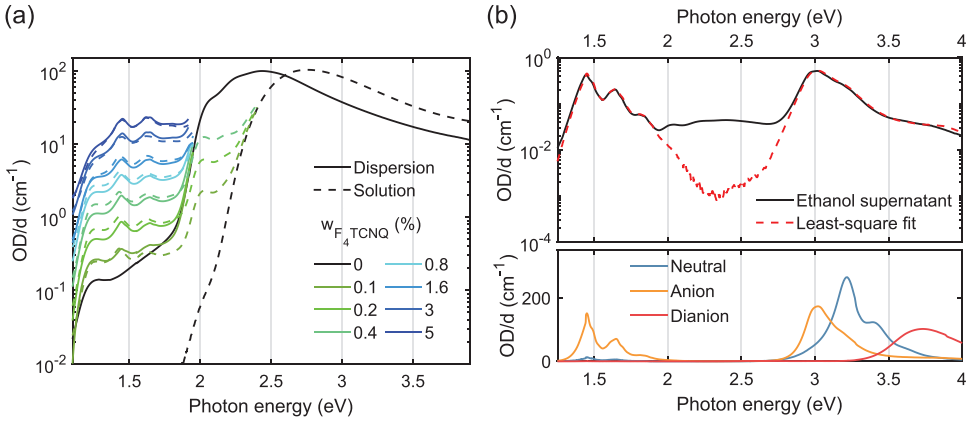

Figure 2. a) Optical densities (per path length) of P3HT dispersions (solid lines) and optical densities of P3HT solutions prior to nanoprecipitation (dashed lines). The measurement of the optical density of doped dispersions and solutions is restricted to the relevant lower photon energies by the experimental setup. b) Top: (Logarithmic) optical density of the ethanol supernatant after coagulation (with sodium bromide) and centrifugation of a P3HT dispersion doped with F_4TCNQ (1 wt%). Traces of P3HT from residual nanoparticles remain visible in the optical density between 2 and 3 eV. The spectrum was deconvolved into the spectra of neutral, anionic, and dianionic F_4TCNQ with a least-square fit. Bottom: Optical densities of neutral F_4TCNQ, F_4TCNQ^- anions, and F_4TCNQ^{2-} dianions (1 g L^{-1} each) for reference [30].

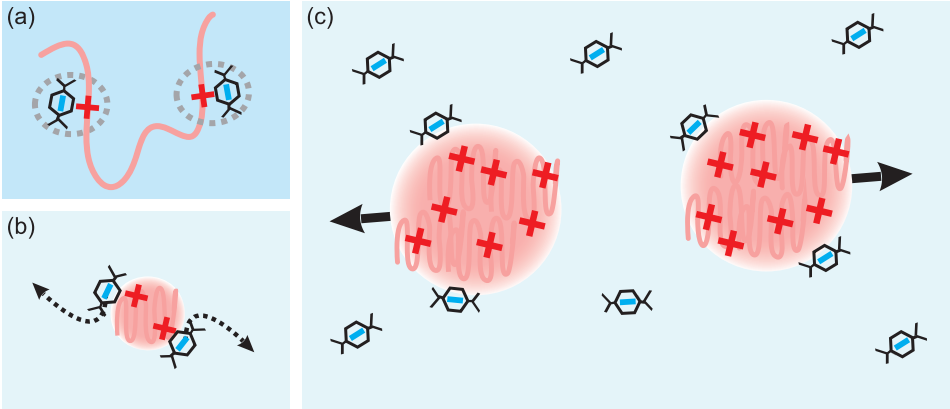

Figure 3. The electrostatic repulsion of organic nanoparticles upon electrical doping of the polymer controls the nanoparticle growth process. a) Upon electrical doping of the polymer in solution with F_4TCNQ, bound ion pairs form. b) During the solvent exchange, the polymer chains collapse into nuclei. The F_4TCNQ^- anions dissociate into the non-solvent ethanol. c) The persisting positive charges on the nanoparticles warrant mutual repulsion of the nanoparticles and therefore, enhance the colloidal stabilization.

Neutral and dianionic states made only negligible contributions to the optical density of the dispersion. Between 2 and 3 eV, we also found traces of P3HT from the remaining nanoparticles. Notably, ethanol solutions of neat F_4TCNQ exhibited different optical densities (for details see Section S3, Supporting Information) as neutral F_4TCNQ tends to react with certain solvents.[41,56] Once in its anionic form, F_4TCNQ appears rather inert against the solvent ethanol. The concentrations of the different F_4TCNQ species in the supernatant add up to 4.0 mg L^{-1}, which equals the amount of F_4TCNQ in the dispersion before the segregation of the particles. This observation suggests that after nanoprecipitation, F_4TCNQ preserves its anionic form and is dissolved in the dispersion medium.

From these findings, we picture the nanoprecipitation process as illustrated in **Figure 3**. The doping of the polymer solution with F_4TCNQ leads to an ion pair of $P3HT^+$ and F_4TCNQ^- (Figure 3a). In a non-polar solvent like chloroform, this ion pair is bound due to the Coulomb attraction of the opposite charges. The solvent exchange causes the formation of polymer nuclei while maintaining the charge distribution (Figure 3b). Due to the high permittivity of ethanol ($\varepsilon_r = 24.5$), the F_4TCNQ^- anions can dissociate from the nanoparticles, leaving a positive charge on the nanoparticles (Figure 3c). This positive charge controls the nanoparticle growth and ultimately leads to enhanced colloidal stability due to the electrostatic repulsion between the nanoparticles. At this stage, without changing the conclusions from this experiment, the distribution of the F_4TCNQ^- anions across the electrical double layer around the nanoparticle remains for further investigation.

2.3. Solar Cells Fabricated from Electrically Doped P3HT:ICBA Nanoparticle Dispersions

After we understood the interaction of P3HT and F_4TCNQ, as well as the corresponding stabilization process of P3HT nanoparticles, we translated our experimental efforts to blends of P3HT:ICBA, which have been used in surfactant-free nanoparticle dispersions for the fabrication of OSCs before.[9,10] Recent reports indicated that the inclusions of fullerenes with residual solubility in the dispersion medium help the dispersion stability by displacing the negative countercharges from the positively charged nanoparticles.[24,57] Earlier investigations on solution-processed polymer:fullerene light-harvesting layers demonstrated no detrimental effects of small amounts of F_4TCNQ on the OSC performance.[28,32,37,42]

We prepared solutions of P3HT:ICBA (1:1 w/w) in chloroform (8 g L^{-1}) and added different amounts of F_4TCNQ (w_{F_4TCNQ} between 0.1 and 1 wt% with respect to the mass of P3HT) to the solutions by injecting the respective amount of F_4TCNQ/acetonitrile solution (10 g L^{-1}). Then we carried out the nanoprecipitation as described in Section 2.1. The dispersions were concentrated to 8 g L^{-1} by thermal evaporation and centrifuged to remove any larger agglomerates, which might later produce defects in the light-harvesting layers. In accordance with the literature, the nanoparticles are likely to exhibit intermixed polymer and fullerene phases due to their rapid formation upon nanoprecipitation. Core–shell architectures, as they are commonly observed in nanoparticles synthesized along the miniemulsion route, require more time to form. **Table 1** summarizes the nanoparticle sizes of the dispersions in dependence on the F_4TCNQ content. Again, we observed that the addition of F_4TCNQ causes a decrease in the nanoparticle size from 76 nm ($w_{F_4TCNQ} = 0$ wt%) to 41 nm ($w_{F_4TCNQ} = 0.4$ wt%). Yet, the effect is not as pronounced as in the previous experiment.

OSCs were fabricated with an inverted device architecture comprising indium tin oxide (ITO)/ZnO/P3HT:ICBA/poly(3,4-ethylenedioxythiophene):polystyrene sulfonate (PEDOT:PSS)/Ag. The P3HT:ICBA layers were spin-coated from dispersions and thermally annealed at 150 °C to merge the nanoparticles for leveling the layers (Figure S4, Supporting Information) and for the best extraction of photo-generated charge carriers, as described previously.[10] During this annealing step, the morphology of the light-harvesting layers may also be reorganized and optimized due to the high diffusivity of the fullerene.[58–60]

The current density–voltage (J–V) curves of representative OSCs are depicted in **Figure 4**a and their key parameters, open-circuit voltage (V_{OC}), short-circuit current (J_{SC}), fill factor (FF),

Table 1. Key parameters of the nanoparticulate P3HT:ICBA solar cells in dependence of the mass ratio of the dopant and the polymer, w_{F_4TCNQ}. Each data set shows the statistics of eight samples (no device failures).

w_{F_4TCNQ} [wt%]	D_{NP}[a)] [nm]	Thickness[b)] [nm]	V_{OC} [mV]	J_{SC} [mA cm^{-2}]	FF [%]	PCE[c)] [%]
0	76	58	851 ± 2	−6.8 ± 0.1	61 ± 1	3.53 ± 0.05 (3.59)
0.1	53	63	835 ± 1	−7.0 ± 0.1	62 ± 1	3.63 ± 0.05 (3.68)
0.2	49	59	830 ± 2	−7.1 ± 0.1	60 ± 2	3.55 ± 0.07 (3.60)
0.4	41	62	810 ± 1	−7.2 ± 0.1	58 ± 1	3.39 ± 0.03 (3.42)
1	68	64	621 ± 6	−6.3 ± 0.1	47 ± 1	1.85 ± 0.03 (1.89)

[a)]Nanoparticle size; [b)]Thickness of the nanoparticulate light harvesting layer; [c)]Hero devices in parentheses.

and PCE are summarized in Table 1. Up to w_{F_4TCNQ} = 0.2 wt%, the incorporation of F_4TCNQ had only a negligible effect on the overall device performance, which is well in accordance with earlier literature reports on the F_4TCNQ-doping of OSCs.[42] J_{SC} gradually increased up to w_{F_4TCNQ} = 0.4 wt%, beyond which it was reduced. The enhanced band at 2 eV of the external quantum efficiency (EQE) (Figure S5, Supporting Information) indicates that the presence of small amounts of F_4TCNQ enhances the crystallinity of P3HT. At w_{F_4TCNQ} = 1 wt% and beyond, a pronounced decrease of the V_{OC} was observed, paired with an overall deterioration of all key parameters.

To investigate the origin of the decrease of the V_{OC} toward higher F_4TCNQ concentrations, we measured the V_{OC} of the respective solar cells in dependence on solar irradiation. Figure 4b depicts the V_{OC} versus the logarithmic irradiance, I, where the V_{OC} follows a linear relation according to:[61]

$$V_{OC} = V_0 - n\frac{k_B T}{e}\cdot\ln\left(\frac{I_0}{I}\right) \quad (1)$$

with the ideality factor n, the Boltzmann constant k_B, the temperature T, the elementary charge e, and the constants I_0 and V_0. An ideality factor close to 1 indicates dominant bimolecular recombination in the device. A larger n indicates a more pronounced Shockley–Read–Hall (SRH) recombination.[62,63] We obtained n = 1.32 for OSCs with neat P3HT:ICBA light-harvesting layers, which is in accordance with earlier literature reports.[64] Upon addition of F_4TCNQ, n gradually increases up to 1.73 (w_{F_4TCNQ} = 0.4 wt%), hence indicating enhanced SRH recombination, which agrees well with the reduction of the V_{OC} and the fill factor toward higher doping ratios. At even higher doping ratios, the developments of the key parameters are much more complex, as discussed in Section S6, Supporting Information. Our observations are well in accordance with previous recombination studies on the influence of dopants on the performance of OSCs.[28,32,65] While small amounts of dopants can reduce SRH recombination by trap filling, the incorporation of large numbers of trap states either intentionally or by impurities can lead to an increased SRH recombination.[63,66,67]

In summary, the incorporation of small amounts of F_4TCNQ into the nanoparticulate solar cells hardly affects the device performance. Only toward larger amounts of F_4TCNQ, we observed minor deterioration of FF and V_{OC}, due to increased recombination. Yet, the simultaneous increase of J_{SC}, presumably due to enhanced absorption, results in an overall increase of the PCE to 3.6% (w_{F_4TCNQ} = 0.1%).

2.4. Dispersions of Other Light-Harvesting Polymers

With the stabilization of polymer nanoparticles mediated by the addition of F_4TCNQ at hand, we now have a tool to investigate the nanoprecipitation of other polymers, which have been inaccessible to the synthesis of surfactant-free nanoparticle inks so far. The high electron affinity of F_4TCNQ (nominal E_{ea} = 5.2 eV[25]) allows p-doping of organic semiconductors with sufficiently low ionization potentials. Therefore, we investigated a variety of organic semiconductors for their principal applicability in

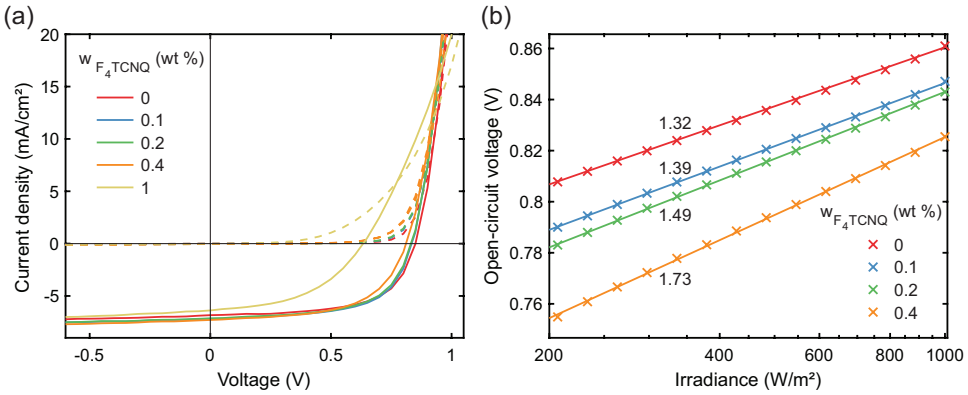

Figure 4. a) J–V curves of nanoparticulate P3HT:ICBA solar cells at different concentrations of F_4TCNQ under 1 sun irradiation (solid lines) and in the dark (dashed lines). b) Open-circuit voltage versus irradiance.

nanoprecipitation. In the first place, we examined the commonly used benzodithiophene-based polymers, poly[[4,8-bis[(2-ethylhexyl)oxy]benzo[1,2-b:4,5-b′]dithiophene-2,6-diyl][3-fluoro-2-[(2-ethylhexyl)carbonyl]thieno[3,4-b]thiophenediyl]] (PTB7), poly[4,8-bis(5-(2-ethylhexyl)thiophen-2-yl)benzo[1,2-*b*;4,5-*b*′]dithiophene-2,6-diyl-alt-(4-(2-ethylhexyl)-3-fluorothieno[3,4-*b*]thiophene-)-2-carboxylate-2-6-diyl)] (PTB7-Th), poly[(2,6-(4,8-bis(5-(2-ethylhexyl)thiophen-2-yl)-benzo[1,2-*b*:4,5-*b*′]dithiophene))-alt-(5,5-(1′,3′-di-2-thienyl-5′,7′-bis(2-ethylhexyl)benzo[1′,2′-*c*:4′,5′-*c*′]dithiophene-4,8-dione)] (PBDB-T), poly[(2,6-(4,8-bis(5-(2-ethylhexyl-3-fluoro)thiophen-2-yl)-benzo[1,2-*b*:4,5-*b*′]dithiophene))-alt-(5,5-(1′,3′-di-2-thienyl-5′,7′-bis(2-ethylhexyl)benzo[1′,2′-*c*:4′,5′-*c*′]dithiophene-4,8-dione)] (PBDB-T-2F), and poly[[5,6-difluoro-2-(2-hexyldecyl)-2*H*-benzotriazole-4,7-diyl]-2,5-thiophenediyl[4,8-bis[5-(tripropylsilyl)-2-thienyl]benzo[1,2-*b*:4,5-*b*′]dithiophene-2,6-diyl]-2,5-thiophenediyl] (J71) as representatives of widely used donor polymers in highly efficient OSCs, all of which do not form nanoparticle dispersions upon nanoprecipitation in the absence of any stabilizing agents.

All polymers were dissolved in chloroform (0.5 g L^{-1}), and F_4TCNQ was added as described above. The polymer solutions were then nanoprecipitated by injecting 1 mL of solution into 4 mL of ethanol. **Figure 5**a shows the nanoparticle sizes 10–20 s after nanoprecipitation. In absence of F_4TCNQ (i.e., $w_{F_4TCNQ} = 0$ wt%), all dispersions coagulated within minutes as exemplified by PTB7 in Figure S8, Supporting Information. Since the nanoparticle sizes of non-stabilized dispersions rapidly increased during the DLS measurements, here, the nanoparticle sizes of dispersions with $w_{F_4TCNQ} = 0$ wt% are provided for orientation only. The addition of F_4TCNQ, however, showed a distinct effect on the nanoparticle formation and colloidal stability. At $w_{F_4TCNQ} = 1$ wt%, the polymers PTB7, PTB7-Th, J71, and PBDB-T formed nanoparticles with average sizes of 100 nm or smaller, further reducing size toward $w_{F_4TCNQ} = 4$ wt%. Notably, a somewhat higher amount of F_4TCNQ was needed to stabilize the dispersions, which can be attributed to a lower doping efficiency of the polymers by F_4TCNQ as rationalized below. The dispersions exhibited shelf stability of several days. Only the colloidal stability of PBDB-T-2F was not enhanced by the addition of F_4TCNQ, but immediate coagulation of the polymer dispersion was observed, which we again attribute to a low doping efficiency.

The effects, which we observed on these polymers, resembled very much the previous findings on the P3HT nanoparticles. Figure 5b depicts the absorption spectrum of PTB7 solutions, which had been doped with different amounts of F_4TCNQ. Again, the addition of F_4TCNQ to the PTB7/chloroform solutions (0.5 g L^{-1}) produces a low-energy absorption shoulder and a peak at 1.45 eV, which is the distinct signature of the F_4TCNQ^- anion. The second peak at 1.65 eV is concealed by the absorption of PTB7. The peak at 1.15 eV can be attributed to the P2 polaron absorption of PTB7.[34,68] But in contrast to P3HT solutions, where almost all F_4TCNQ was reduced to the anionic F_4TCNQ^-, most of F_4TCNQ remained in the neutral state as became visible in the characteristic absorption peaks at 3.2 and 3.4 eV. We conclude that only a small fraction of F_4TCNQ engages in the oxidation of the polymer,[34] and therefore, a higher concentration of F_4TCNQ was needed to push the chemical equilibrium toward sufficient amounts of charges to stabilize the dispersion. Apparently, the doping efficiency of F_4TCNQ on PTB7 is much lower, which is probably why F_4TCNQ has never been reported as a dopant for PTB7 before. Consequently, the amount of F_4TCNQ that is required to stabilize the PTB7 dispersion, is much higher than for P3HT.[38,40,69]

2.5. Solar Cells Fabricated from PTB7:$PC_{71}BM$ Dispersions

In order to fabricate solar cells from PTB7 dispersions, the concentration of the nanoparticle dispersions must be increased (>1 g L^{-1}) by thermal evaporation of chloroform and substantial amounts of non-solvent. The low doping efficiency of F_4TCNQ on PTB7 opens up a competing process during the formation of the dispersion. In its neutral state, F_4TCNQ can react with ethanol, as discussed in Section S3, Supporting Information, with the effect being more pronounced at elevated temperatures, for example, during the concentration of the dispersion. This competing process hinders F_4TCNQ from doping PTB7[41] and hence, reduces the charging of the nanoparticles. Therefore, in this experiment, we opted for acetonitrile as the non-solvent (i.e., the dispersion medium, $\varepsilon_r = 37.5$), which is inert against reaction with F_4TCNQ,[41] and which allowed us the thermal removal of the chloroform and the concentration of the dispersion.

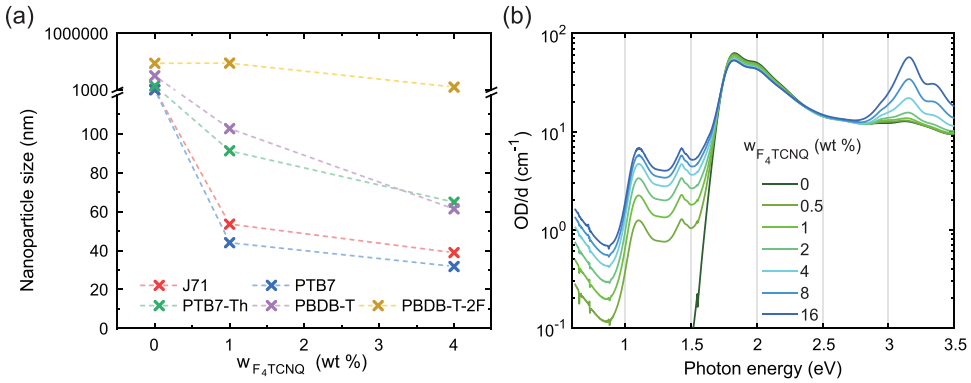

Figure 5. a) Nanoparticle sizes of polymer dispersions of J71, PTB7, PTB7-Th, PBDB-T, or PBDB-T-2F in ethanol versus the amount of F_4TCNQ. Dotted lines are drawn to guide the eye. b) Optical densities of PTB7/chloroform solutions (0.5 g L^{-1}) doped with F_4TCNQ. The two peaks at 3.2 and 3.4 eV can be attributed to F_4TCNQ in its neutral state. They increase for larger amounts of F_4TCNQ. Anionic F_4TCNQ^- shows a characteristic peak at 1.45 eV.

Table 2. Key parameters of the nanoparticulate PTB7:$PC_{71}BM$ solar cells. Each data set shows the statistics of eight samples (no device failures).

w_{F_4TCNQ} [w%]	D_{NP}[a)] [nm]	Thickness[b)] [nm]	V_{OC} [mV]	J_{SC} [mA cm^{-2}]	FF [%]	PCE[c)] [%]
20	97	80	790 ± 10	−6.4 ± 0.1	29 ± 1	1.5 ± 0.1 (1.5)
40	89	90	780 ± 10	−5.3 ± 0.1	28 ± 1	1.2 ± 0.1 (1.2)

[a)]Nanoparticle size; [b)]Thickness of the nanoparticulate light harvesting layer; [c)]Hero devices in parentheses

For the fabrication of solar cells, we chose to combine PTB7 with the fullerene acceptor $PC_{71}BM$ (1:1 w/w). F_4TCNQ (20 or 40 wt% with respect to the mass of PTB7) was added to PTB7:$PC_{71}BM$/chloroform solutions (2 g L^{-1}) and the solutions were nanoprecipitated in an excess of seven parts of acetonitrile. The significantly larger amount of F_4TCNQ is a direct consequence of the much lower doping efficiency as discussed above. The dispersions were concentrated to 1 g L^{-1} by thermal evaporation and centrifuged to remove any larger agglomerates, which otherwise might later produce defects in the light-harvesting layers. Similar to neat PTB7 dispersions, in absence of F_4TCNQ, the PTB7:$PC_{71}BM$ dispersions immediately coagulated and sedimented.

In the next step, the light-harvesting layers were spin-cast from the nanoparticle dispersions, thermally annealed, and integrated into solar cells with regular device architecture (Glass/ITO/PEDOT:PSS/PTB7:$PC_{71}BM$/ZnO/Ag). AFM micrographs of the nanoparticulate PTB7:$PC_{71}BM$ layers are depicted in Figure S4, Supporting Information. The respective key parameters are summarized in **Table 2**, and the *J*–*V* curves are depicted in **Figure 6**. Both batches of solar cells exhibit low fill factors accompanied by a moderate J_{SC}, altogether producing PCEs of 1.2% or 1.5%. We observed a strong voltage dependence of the device current under reverse bias, attributable to a field dependence of the charge carrier generation. Hence, the origin of the moderate device performance is likely a non-optimized bulk-heterojunction morphology.[70] Similar performance deteriorations have been reported for PTB7:$PC_{71}BM$ solar cells processed from solution, whenever omitting solvent additives.[71–73]

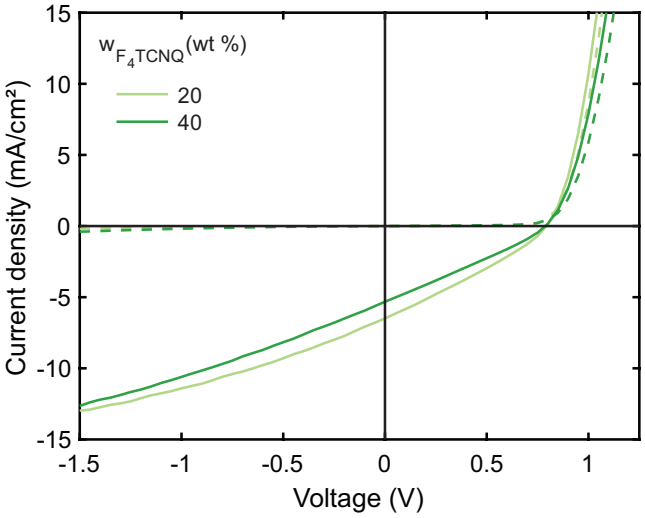

Figure 6. Representative *J*–*V* curves of nanoparticulate PTB7:$PC_{71}BM$ solar cells (w_{F_4TCNQ} = 20, 40 wt%) under 1 sun irradiation (solid lines) and in the dark (dashed lines).

In contrast to P3HT:fullerene solar cells, where the morphology can be controlled by thermal annealing,[74–76] the use of solvent additives for the fabrication of PTB7:fullerene bulk-heterojunctions is compulsory to reach favorable morphologies (see also the comparison of the AFM micrographs before and after thermal annealing in Figure S4, Supporting Information). Yet, so far, solvent additives are not readily compatible with nanoparticle formation by nanoprecipitation.

3. Conclusions

The electrical doping of semiconducting polymers by the introduction of the strong electron acceptor F_4TCNQ to the nanoprecipitation allows the electrostatic stabilization of dispersions and the precise control of nanoparticle sizes. We have demonstrated this novel concept in the formation of P3HT and P3HT:ICBA dispersions. We used lowest F_4TCNQ concentrations to tailor the P3HT nanoparticle size in the range of 25–75 nm. Importantly, the performance of the corresponding solar cells comprising light-harvesting layers fabricated from these dispersions is hardly affected by the addition of small amounts of F_4TCNQ. Our process can be readily transferred to the electrostatic stabilization of several benzodithiophene copolymer dispersions, among them the widely used PTB7 and its derivatives, significantly broadening the future choice of organic semiconductors for nanoparticulate solar cells. Although the performances of the corresponding PTB7:$PC_{71}BM$ solar cells do not live up to other reports due to lacking morphology control, we consider our study a blueprint for future stabilization of nanoparticle dispersions. By choosing suitable strong acceptors, dispersions of organic semiconductors can be stabilized omitting surfactants, which are commonly considered detrimental to the device performance. At the same time, this study calls for distinct efforts in the design of organic semiconductors to be processed from eco-friendly nanoparticle dispersions. Today, all light-harvesting polymers are designed to yield good bulk-heterojunction morphologies when processed from solution, but morphology control for best PCEs on the nanoparticle route apparently requires other, yet-to-be-specified, sets of material properties.

4. Experimental Section

Materials: P3HT ("4002-EE," M_w = 50–70 kg mol^{-1}, regioregularity > = 90%) was purchased from Rieke Metals; ICBA from Solenne; PTB7, PTB7-Th, PBDB-T and PBTB-T-2F from 1-Material; F_4TCNQ from Ossila. All organic semiconductors were used as received without further purification and stored under a nitrogen atmosphere.

Ethanol (absolute, Emsure), acetonitrile, and chloroform (all analytical grade) were purchased from Merck and used without further purification. Notably, ethanol batch variations could affect the

nanoparticle formation, influencing the nanoparticle size and colloidal stability of the dispersion.

Preparation of Semiconductor Solutions: All semiconductors were dissolved separately in chloroform (0.5–8 g L^{-1}) before use and stirred for at least 20 min under ambient conditions. Donor/acceptor blend solutions were prepared by mixing the individual solutions in equal volumes.

Doping of Organic Semiconductor Solutions: F_4TCNQ was dissolved in acetonitrile (10 g L^{-1}) at room temperature. The stock solutions were stirred before use (1 h). Solutions of F_4TCNQ with low concentrations, which were used to yield low doping ratios, were achieved by dilution of the F_4TCNQ stock solution with acetonitrile. The semiconductor solutions were then doped by adding the required amount of F_4TCNQ in acetonitrile solution to the organic semiconductor solution, thereby negligibly diluting the solution by less than 1 vol%, even at high doping ratios. The doped semiconductor solutions were heated (50 °C, 10–30 min) to avoid pre-agglomeration in the solution. F_4TCNQ slowly reacts with ethanol (see Section S3, Supporting Information) and hence, F_4TCNQ was deactivated within hours after dissolution in ethanol (or in ethanol-stabilized chloroform), which prompted the use of acetonitrile to initially dissolve F_4TCNQ. Yet, after charge transfer from the organic semiconductor, the F_4TCNQ^- anion was inert against ethanol.

Nanoparticle Synthesis: Organic nanoparticle dispersions were prepared by nanoprecipitation. Therefore, beakers with the non-solvent (ethanol or acetonitrile, 4 mL) were heated on a hotplate (50 °C). The organic semiconductor solutions were then injected into the non-solvent (P3HT, P3HT:ICBA, PTB7, PTB7-Th, J71 PBDB-T, and PBDB-T-2F into ethanol: 1:4 v/v; PTB7:$PC_{71}BM$ into acetonitrile: 1:7 v/v) under stirring. The good miscibility of solvent and non-solvent led to an immediate reduction of semiconductor solubility and hence to the formation of nanoparticles.

Investigation of F_4TCNQ in the Non-Solvent: A solution of P3HT:F_4TCNQ (99:1 w/w) in chloroform (2 g L^{-1}) was nanoprecipitated in ethanol (1:4 v/v) and coagulated by the addition of sodium bromide (10^{-3} M) afterward. Then, the agglomerates were removed by centrifugation (Eppendorf, MiniSpin plus, 14 500 rpm, 14 100g, 2 min). The remaining components in ethanol were differentiated by deconvolving the optical density of the supernatant into contributions from 1) neutral F_4TCNQ, 2) anions, 3) dianions, and 4) the reaction product of F_4TCNQ in ethanol using least-square fits.

Fabrication of P3HT:ICBA Organic Solar Cells: The nanoparticle dispersions were nanoprecipitated by injecting P3HT:ICBA (1:1 w/w) chloroform solutions (8 g L^{-1}) into ethanol (1:4 v/v) as described above. The concentrations of the dispersions were increased and the remaining chloroform in the dispersions was removed by evaporation (70 °C) until their volumes were reduced to the volume of the initial P3HT:ICBA solutions (8 g L^{-1}). Afterward, contingent agglomerates were removed by centrifugation. The concentrations of the resulting dispersions were monitored in absorbance measurements and compared to reference spectra by least-square fits.

Solar cells were fabricated with inverted device architecture. ITO-covered glass substrates were cleaned by wiping with cleanroom tissues and isopropanol and subsequently ultrasonicated in acetone and isopropanol (10 min each). Visible remaining particles were removed by a cleanroom polyester swab and isopropanol. All subsequent steps were carried out under inert conditions (<10 ppm oxygen, <10 ppm water). Electron transport layers (10 nm) were spin-cast (2000 rpm, 40 s) from zinc oxide nanoparticles (1 wt%, in butanol)[77] and dried on a hotplate (120 °C, 10 min). The light-harvesting layers were then applied by three subsequent spin coating steps. The spin coating speeds (2600–2900 rpm) were individually adjusted to yield the same layer thicknesses (60 nm) in all experiments. The samples were then annealed on a hotplate (150 °C, 10 min). For the deposition of the hole transport layers, PEDOT:PSS (HTL Solar, Heraeus) was filtered (pore size: 0.45 µm), diluted with water (1:1 v/v), spin-cast (500 rpm, 3 s; 2000 rpm, 40 s; 30 nm) and annealed on a hotplate (120 °C, 10 min). Finally, the silver top electrodes (100 nm) were sublimed in high vacuum (base pressure $\leq 1 \times 10^{-6}$ mbar).

Fabrication of PTB7:$PC_{71}BM$ Organic Solar Cells: The nanoparticle dispersions were nanoprecipitated by injecting PTB7:$PC_{71}BM$ (1:1 w/w) chloroform solutions (2 g L^{-1}) into acetonitrile (1:7 v/v) as described above. The concentrations of the dispersions were increased and the remaining chloroform in the dispersions was removed by evaporation (70 °C) until their volumes were reduced to twice the volume of the initial PTB7:$PC_{71}BM$ solution (1 g L^{-1}). Afterward, contingent agglomerates were removed by centrifugation and the concentrations of the resulting dispersions were monitored in absorbance as described above.

Solar cells were fabricated with regular device architecture on glass/ITO substrates that were cleaned as described above. The substrates were treated with an oxygen plasma (2 min). PEDOT:PSS (VPAI 4083, Heraeus) was filtered (pore size: 0.45 µm), spin-cast (5000 rpm, 30 s) on the samples under ambient conditions, and dried on a hotplate (150 °C, 10 min). All subsequent steps were carried out under inert conditions (<10 ppm oxygen, <10 ppm water). The light-harvesting layers were then applied by 20 subsequent spin coating steps (800 rpm, 10 s). The number of spin coating steps was adjusted to ensure equal layer thicknesses (100 nm). The samples were then annealed on a hotplate (180 °C, 10 min). Electron transport layers were spin-cast (1000 rpm, 40 s) from zinc oxide nanoparticles (1 wt%, in butanol) and dried on a hotplate (120 °C, 10 min). Finally, the silver top electrodes (100 nm) were sublimed in high vacuum (base pressure $\leq 1 \times 10^{-6}$ mbar).

Optical Density Measurement: The optical density of solutions and dispersions was recorded in double-beam mode with a UV–vis-NIR spectrophotometer (Agilent Cary 5000). The samples were measured in a quartz cuvette against the respective solvent or dispersion medium, neglecting any addition of acetonitrile (<1 vol%). For the optical density measurements of doped P3HT/chloroform solutions (2 g L^{-1}), the samples were not diluted in order to avoid changes in the doping rate.[35] For the optical density measurements of dispersions, identical solutions were nanoprecipitated in ethanol, reducing the concentration to 0.4 g L^{-1}, and again measured without further dilution. To compare the solutions with the dispersions, the absorbance of the dispersions was multiplied by 5. The optical density measurements of PTB7 solutions were carried out at 0.5 g L^{-1}. Cuvettes of different optical path lengths (1 and 10 mm) were used to capture the optical density per path length over several orders of magnitude.

Nanoparticle Size Measurement: The intensity-based average nanoparticle sizes of dispersions were measured via dynamic light scattering (Malvern Panalytical, Zetasizer Nano ZS). Small amounts of the dispersions (10 µL) were diluted with ethanol (1 mL) in a polystyrene cuvette and characterized by 15 consecutive runs, 10 s each. Extreme outliers were removed from the statistical analysis.

Solar Cell Characterization: The solar cells were measured under standard conditions (1 sun, AM 1.5G) in a nitrogen atmosphere. AM 1.5G was simulated with a xenon high-pressure solar simulator (Sciencetech, Lightline AX-LA200, Classification AAA, ASTM E927), and its power was adjusted to 1 sun by a silicon reference solar cell with a KG5 filter (Newport 91150-KG5). The electric characteristics were obtained by a current–voltage sweep from –1.5 to 1.5 V with a source meter unit (Keithley 2420) in 4-wire mode. The spectral mismatch factors were determined by measuring the EQE of each solar cell variation according to ASTM E973 without tracking the temperature difference and used to calculate corrected currents.

For the illumination-intensity-dependent open-circuit voltage measurements, the current was set to zero and different solar irradiations were generated by adjusting the output levels of an LED solar simulator (Newport, Oriel Verasol-2, Classification AAA, ASTM E927). The spectra were monitored with an array-spectrometer (Instrument Systems CAS 140CT-156 with EOP-146 optics).

External Quantum Efficiency: The wavelength-dependent EQEs of the solar cells were measured with a home-built setup. A xenon high-pressure lamp (450W LSH601, LOT Oriel) was used to generate broadband white light. A Czerny–Turner-monochromator (Omni-λ300, LOT Oriel with an MSZ3122, LOT Oriel filter wheel) was used to sequentially select monochromatic light. To allow for lock-in amplification, the light was optically chopped (C-995, Terahertz

Technologies) at 373 Hz. To track fluctuations of the xenon high-pressure lamp, the output light was split into two beams. The first beam was focused on a monitor photodiode (K1713-09, Hamamatsu). The second beam was coupled into an optical fiber (fiber patch cable M37L02, Thorlabs), which led into a nitrogen glovebox to measure in inert conditions. The light was decoupled and focused onto the measurement sample. Two transimpedance amplifiers (OE-200S, Femto Messtechnik) were used to convert the current into an amplified voltage. The voltage signal was measured by a lock-in amplifier (eLockIn 203, Anfatec Instruments) with a settling time of 2 s and 2 s integration time. The setup was referenced to a calibrated photodiode (818-UV-20925, Newport Corporation, calibrated per procedure no PTP99163 by Newport Corporation in December 2020 with traceability no O-0000000544) to obtain the spectral response.

Supporting Information

Supporting Information is available from the Wiley Online Library or from the author.

Acknowledgements

This work was financed by the German Ministry of Education and Research (BMBF) under contract no. 03EK3571 (project TAURUS II) and later by the Helmholtz research program "Materials and Technologies for the Energy Transition (MTET)." K.F. received funding from the Graduate School for Climate and Environment (GRACE). The authors thank Andreas Tangemann (KIT), Holger Röhm (KIT), and David Jones (The University of Melbourne) for fruitful discussions. The authors acknowledge Kiefer et al. for providing the raw data of the absorbance of the different F_4TCNQ species from their earlier work.

Open access funding enabled and organized by Projekt DEAL.

Conflict of Interest

The authors declare no conflict of interest.

Data Availability Statement

The data that support the findings of this study are available from the corresponding author upon reasonable request.

Keywords

electrical doping, electrostatic stabilization, nanoprecipitation, organic nanoparticles, organic solar cells

Received: March 4, 2022
Revised: April 22, 2022
Published online: June 8, 2022

[1] R. K. Henderson, C. Jiménez-González, D. J. C. Constable, S. R. Alston, G. G. A. Inglis, G. Fisher, J. Sherwood, S. P. Binks, A. D. Curzons, *Green Chem.* **2011**, *13*, 854.
[2] K. Alfonsi, J. Colberg, P. J. Dunn, T. Fevig, S. Jennings, T. A. Johnson, H. P. Kleine, C. Knight, M. A. Nagy, D. A. Perry, M. Stefaniak, *Green Chem.* **2008**, *10*, 31.
[3] D. Prat, O. Pardigon, H.-W. Flemming, S. Letestu, V. Ducandas, P. Isnard, E. Guntrum, T. Senac, S. Ruisseau, P. Cruciani, P. Hosek, *Org. Process Res. Dev.* **2013**, *17*, 1517.
[4] A. Anctil, E. Lee, R. R. Lunt, *Appl. Energy* **2020**, *261*, 114429.
[5] A. Colsmann, H. Röhm, C. Sprau, *Sol. RRL* **2020**, *4*, 2000015.
[6] H. Chen, H. Lai, Z. Chen, Y. Zhu, H. Wang, L. Han, Y. Zhang, F. He, *Angew. Chem., Int. Ed.* **2021**, *60*, 3238.
[7] W. Guan, D. Yuan, J. Wu, X. Zhou, H. Zhao, F. Guo, L. Zhang, K. Zhou, W. Ma, W. Cai, J. Chen, L. Ding, L. Hou, W. Guan, D. Yuan, J. T. Wu, X. B. Zhou, H. Zhao, F. Guo, L. J. Zhang, K. Zhou, W. Ma, Z. Cai, J. W. Chen, L. M. Ding, L. T. Hou, *J. Semicond.* **2021**, *42*, 030502.
[8] D. Wang, G. Zhou, Y. Li, K. Yan, L. Zhan, H. Zhu, X. Lu, H. Chen, C.-Z. Li, D. Wang, K. Yan, L. Zhan, H. Chen, C.-Z. Li, G. Zhou, H. Zhu, Y. Li, X. Lu, *Adv. Funct. Mater.* **2021**, *32*, 2107827.
[9] S. Sankaran, K. Glaser, S. Gärtner, T. Rödlmeier, K. Sudau, G. Hernandez-Sosa, A. Colsmann, *Org. Electron.* **2016**, *28*, 118.
[10] S. Gärtner, M. Christmann, S. Sankaran, H. Röhm, E.-M. Prinz, F. Penth, A. Pütz, A. E. Türeli, B. Penth, B. Baumstümmler, A. Colsmann, *Adv. Mater.* **2014**, *26*, 6653.
[11] C. Wu, B. Bull, C. Szymanski, K. Christensen, J. McNeill, *ACS Nano* **2008**, *2*, 2415.
[12] S. Ulum, N. Holmes, D. Darwis, K. Burke, A. L. David Kilcoyne, X. Zhou, W. Belcher, P. Dastoor, *Sol. Energy Mater. Sol. Cells* **2013**, *110*, 43.
[13] X. Pan, A. Sharma, D. Gedefaw, R. Kroon, A. Diaz de Zerio, N. P. Holmes, A. L. D. Kilcoyne, M. G. Barr, A. Fahy, M. Marks, X. Zhou, W. Belcher, P. C. Dastoor, M. R. Andersson, *Org. Electron.* **2018**, *59*, 432.
[14] F. J. M. Colberts, M. M. Wienk, R. A. J. Janssen, *ACS Appl. Mater. Interfaces* **2017**, *9*, 13380.
[15] D. Darwis, N. Holmes, D. Elkington, A. L. David Kilcoyne, G. Bryant, X. Zhou, P. Dastoor, W. Belcher, *Sol. Energy Mater. Sol. Cells* **2014**, *121*, 99.
[16] C. Xie, A. Classen, A. Späth, X. Tang, J. Min, M. Meyer, C. Zhang, N. Li, A. Osvet, R. H. Fink, C. J. Brabec, *Adv. Energy Mater.* **2018**, *8*, 1702857.
[17] C. Xie, T. Heumüller, W. Gruber, X. Tang, A. Classen, I. Schuldes, M. Bidwell, A. Späth, R. H. Fink, T. Unruh, I. McCulloch, N. Li, C. J. Brabec, *Nat. Commun.* **2018**, *9*, 5335.
[18] M. G. Barr, S. Chambon, A. Fahy, T. W. Jones, M. A. Marcus, A. L. D. Kilcoyne, P. C. Dastoor, M. J. Griffith, N. P. Holmes, *Mater. Chem. Front.* **2021**, *5*, 2218.
[19] H. Takeuchi, M. Kobashi, *Chem. Lett.* **1999**, *28*, 415.
[20] H. Shimizu, M. Yamada, R. Wada, M. Okabe, *Polym. J.* **2007**, *40*, 33.
[21] J. Schneider, M. K. Meinel, H. Dittmar, F. Müller-Plathe, *Macromolecules* **2020**, *53*, 8889.
[22] S. Gärtner, A. J. Clulow, I. A. Howard, E. P. Gilbert, P. L. Burn, I. R. Gentle, A. Colsmann, *ACS Appl. Mater. Interfaces* **2017**, *9*, 42986.
[23] Z. Zhu, N. Xu, Q. Yu, L. Guo, H. Cao, X. Lu, Y. Cai, *Macromol. Rapid Commun.* **2015**, *36*, 1521.
[24] P. Marlow, F. Manger, K. Fischer, C. Sprau, A. Colsmann, *Nanoscale* **2022**, *14*, 5569.
[25] W. Gao, A. Kahn, *Appl. Phys. Lett.* **2001**, *79*, 4040.
[26] J. Gao, J. D. Roehling, Y. Li, H. Guo, A. J. Moulé, J. K. Grey, *J. Mater. Chem. C* **2013**, *1*, 5638.
[27] I. E. Jacobs, E. W. Aasen, J. L. Oliveira, T. N. Fonseca, J. D. Roehling, J. Li, G. Zhang, M. P. Augustine, M. Mascal, A. J. Moulé, *J. Mater. Chem. C* **2016**, *4*, 3454.
[28] Z. Shang, T. Heumueller, R. Prasanna, G. F. Burkhard, B. D. Naab, Z. Bao, M. D. McGehee, A. Salleo, *Adv. Energy Mater.* **2016**, *6*, 1601149.

[29] T. Schneider, F. Limberg, K. Yao, A. Armin, N. Jürgensen, J. Czolk, B. Ebenhoch, P. Friederich, W. Wenzel, J. Behrends, H. Krüger, A. Colsmann, *J. Mater. Chem. C* **2017**, *5*, 770.
[30] D. Kiefer, R. Kroon, A. I. Hofmann, H. Sun, X. Liu, A. Giovannitti, D. Stegerer, A. Cano, J. Hynynen, L. Yu, Y. Zhang, D. Nai, T. F. Harrelson, M. Sommer, A. J. Moulé, M. Kemerink, S. R. Marder, I. McCulloch, M. Fahlman, S. Fabiano, C. Müller, *Nat. Mater.* **2019**, *18*, 149.
[31] J. H. Burke, M. J. Bird, *Adv. Mater.* **2019**, *31*, 1806863.
[32] Y. Xiong, L. Ye, A. Gadisa, Q. Zhang, J. J. Rech, W. You, H. Ade, *Adv. Funct. Mater.* **2019**, *29*, 1806262.
[33] M. G. Voss, D. T. Scholes, J. R. Challa, B. J. Schwartz, *Faraday Discuss.* **2019**, *216*, 339.
[34] M. G. Voss, J. Reddy Challa, D. Tyler Scholes, P. Y. Yee, E. C. Wu, X. Liu, S. J. Park, O. León Ruiz, S. Subramaniyan, M. D. Chen, S. A. Jenekhe, X. L. Wang, S. H. Tolbert, B. J. Schwartz, M. G. Voss, J. R. Challa, D. T. Scholes, P. Y. Yee, E. C. Wu, X. Liu, S. J. Park, O. León Ruiz, X. L. Wang, S. H. Tolbert, B. J. Schwartz, S. Subramaniyan, S. A. Jenekhe, M. D. Chen, et al., *Adv. Mater.* **2021**, *33*, 2000228.
[35] P. Pingel, D. Neher, *Phys. Rev. B* **2013**, *87*, 115209.
[36] X. Han, Z. Wu, B. Sun, *Org. Electron.* **2013**, *14*, 1116.
[37] Y. Zhang, H. Zhou, J. Seifter, L. Ying, A. Mikhailovsky, A. J. Heeger, G. C. Bazan, T.-Q. Nguyen, *Adv. Mater.* **2013**, *25*, 7038.
[38] F. Ghani, A. Opitz, P. Pingel, G. Heimel, I. Salzmann, J. Frisch, D. Neher, A. Tsami, U. Scherf, N. Koch, *J. Polym. Sci. B. Polym. Phys.* **2015**, *53*, 58.
[39] C. Wang, D. T. Duong, K. Vandewal, J. Rivnay, A. Salleo, *Phys. Rev. B* **2015**, *91*, 85205.
[40] D. Di Nuzzo, C. Fontanesi, R. Jones, S. Allard, I. Dumsch, U. Scherf, E. von Hauff, S. Schumacher, E. Da Como, *Nat. Commun.* **2015**, *6*, 6460.
[41] J. Fuzell, I. E. Jacobs, S. Ackling, T. F. Harrelson, D. M. Huang, D. Larsen, A. J. Moulé, *J. Phys. Chem. Lett.* **2016**, *7*, 4297.
[42] H. Yan, J. G. Manion, M. Yuan, F. P. G. de Arquer, G. R. McKeown, S. Beaupré, M. Leclerc, E. H. Sargent, D. S. Seferos, *Adv. Mater.* **2016**, *28*, 6491.
[43] T. I. Morozova, A. Nikoubashman, *J. Phys. Chem. B* **2018**, *122*, 2130.
[44] C. Zhang, V. J. Pansare, R. K. Prud'homme, R. D. Priestley, *Soft Matter* **2011**, *8*, 86.
[45] N. Li, A. Nikoubashman, A. Z. Panagiotopoulos, *J. Chem. Phys.* **2018**, *149*, 084904.
[46] E. J. W. Verwey, *J. Phys. Colloid Chem.* **1947**, *51*, 631.
[47] J. Polte, *CrystEngComm* **2015**, *17*, 6809.
[48] A. Nikoubashman, V. E. Lee, C. Sosa, R. K. Prud'homme, R. D. Priestley, A. Z. Panagiotopoulos, *ACS Nano* **2016**, *10*, 1425.
[49] D. T. Scholes, P. Y. Yee, J. R. Lindemuth, H. Kang, J. Onorato, R. Ghosh, C. K. Luscombe, F. C. Spano, S. H. Tolbert, B. J. Schwartz, *Adv. Funct. Mater.* **2017**, *27*, 1702654.
[50] O. Inganäs, W. R. Salaneck, J. Österholm, J. Laakso, *Synth. Met.* **1988**, *22*, 395.
[51] C. Scharsich, R. H. Lohwasser, M. Sommer, U. Asawapirom, U. Scherf, M. Thelakkat, D. Neher, A. Köhler, *J. Polym. Sci. B. Polym. Phys.* **2012**, *50*, 442.
[52] S. Sweetnam, K. R. Graham, G. O. N. Ndjawa, T. Heumüller, J. A. Bartelt, T. M. Burke, W. Li, W. You, A. Amassian, M. D. McGehee, *J. Am. Chem. Soc.* **2014**, *136*, 14078.
[53] C. Enengl, S. Enengl, S. Pluczyk, M. Havlicek, M. Lapkowski, H. Neugebauer, E. Ehrenfreund, *ChemPhysChem* **2016**, *17*, 3836.
[54] K. Rahimi, I. Botiz, J. O. Agumba, S. Motamen, N. Stingelin, G. Reiter, *RSC Adv.* **2014**, *4*, 11121.
[55] F. C. Spano, C. Silva, *Annu. Rev. Phys. Chem.* **2014**, *65*, 477.
[56] K. Tanemura, Y. Nishida, T. Suzuki, K. Satsumabayashi, T. Horaguchi, *J. Chem. Res.* **1999**, 40.
[57] A. Palacio Valera, C. Schatz, E. Ibarboure, T. Kubo, H. Segawa, S. Chambon, *Front. Energy Res.* **2019**, *6*, 146.
[58] B. A. Collins, J. R. Tumbleston, H. Ade, *J. Phys. Chem. Lett.* **2011**, *2*, 3135.
[59] D. Chen, F. Liu, C. Wang, A. Nakahara, T. P. Russell, *Nano Lett.* **2011**, *11*, 2071.
[60] N. D. Treat, M. A. Brady, G. Smith, M. F. Toney, E. J. Kramer, C. J. Hawker, M. L. Chabinyc, *Adv. Energy Mater.* **2011**, *1*, 82.
[61] W. Tress, M. Yavari, K. Domanski, P. Yadav, B. Niesen, J. P. C. Baena, A. Hagfeldt, M. Graetzel, *Energy Environ. Sci.* **2018**, *11*, 151.
[62] G.-J. A. H. Wetzelaer, L. J. A. Koster, P. W. M. Blom, *In Organic Photovoltaics* (Eds: C. Brabec, U. Scherf), Wiley-VCH, Weinheim, Germany, **2014**, pp. 343.
[63] S. R. Cowan, W. L. Leong, N. Banerji, G. Dennler, A. J. Heeger, *Adv. Funct. Mater.* **2011**, *21*, 3083.
[64] S. Yan, L. Lv, Y. Ning, L. Qin, C. Li, X. Liu, Y. Hu, Z. Lou, F. Teng, Y. Hou, *Phys. Status Solidi A* **2015**, *212*, 2169.
[65] Y. Lin, Y. Firdaus, M. I. Nugraha, F. Liu, S. Karuthedath, A. H. Emwas, W. Zhang, A. Seitkhan, M. Neophytou, H. Faber, E. Yengel, I. McCulloch, L. Tsetseris, F. Laquai, T. D. Anthopoulos, *Adv. Sci.* **2020**, *7*, 1903419.
[66] M. M. Mandoc, F. B. Kooistra, J. C. Hummelen, B. de Boer, P. W. M. Blom, *Appl. Phys. Lett.* **2007**, *91*, 263505.
[67] W. L. Leong, G. C. Welch, L. G. Kaake, C. J. Takacs, Y. Sun, G. C. Bazan, A. J. Heeger, *Chem. Sci.* **2012**, *3*, 2103.
[68] S. Baniya, S. R. Vardeny, E. Lafalce, N. Peygambarian, Z. V. Vardeny, *Phys. Rev. Appl.* **2017**, *7*, 064031.
[69] I. Salzmann, G. Heimel, *J. Electron Spectrosc. Relat. Phenom.* **2015**, *204*, 208.
[70] J. Kniepert, I. Lange, J. Heidbrink, J. Kurpiers, T. J. K. Brenner, L. J. A. Koster, D. Neher, *J. Phys. Chem. C* **2015**, *119*, 8310.
[71] N. Jain, N. Chandrasekaran, A. Sadhanala, R. H. Friend, C. R. McNeill, D. Kabra, *J. Mater. Chem. A* **2017**, *5*, 24749.
[72] Y. Liang, Z. Xu, J. Xia, S.-T. Tsai, Y. Wu, G. Li, C. Ray, L. Yu, *Adv. Mater.* **2010**, *22*, E135.
[73] C. Sprau, F. Buss, M. Wagner, D. Landerer, M. Koppitz, A. Schulz, D. Bahro, W. Schabel, P. Scharfer, A. Colsmann, *Energy Environ. Sci.* **2015**, *8*, 2744.
[74] T. Erb, U. Zhokhavets, G. Gobsch, S. Raleva, B. Stühn, P. Schilinsky, C. Waldauf, C. J. Brabec, *Adv. Funct. Mater.* **2005**, *15*, 1193.
[75] G. Li, V. Shrotriya, J. Huang, Y. Yao, T. Moriarty, K. Emery, Y. Yang, *Nat. Mater.* **2005**, *4*, 864.
[76] G. Li, V. Shrotriya, Y. Yao, J. Huang, Y. Yang, *J. Mater. Chem.* **2007**, *17*, 3126.
[77] B. Sun, H. Sirringhaus, *Nano Lett.* **2005**, *5*, 2408.